QUANTUM PHYSICS

Tweezer-programmable 2D quantum walks in a Hubbard-regime lattice

Aaron W. Young¹, William J. Eckner¹, Nathan Schine¹, Andrew M. Childs^{2,3}, Adam M. Kaufman¹*

Quantum walks provide a framework for designing quantum algorithms that is both intuitive and universal. To leverage the computational power of these walks, it is important to be able to programmably modify the graph a walker traverses while maintaining coherence. We do this by combining the fast, programmable control provided by optical tweezers with the scalable, homogeneous environment of an optical lattice. With these tools we study continuous-time quantum walks of single atoms on a square lattice and perform proof-of-principle demonstrations of spatial search with these walks. When scaled to more particles, the capabilities demonstrated can be extended to study a variety of problems in quantum information science, including performing more effective versions of spatial search using a larger graph with increased connectivity.

he ability of quantum systems to coherently explore their Hilbert space, exhibiting wavelike superposition and interference, is a key ingredient in quantum algorithms. Quantum walks are one intuitive framework for understanding the algorithmic speedups that these ingredients can provide. In this framework, states in Hilbert space are mapped to the locations of a walker on a graph (*I*); the walker can then traverse this graph through a superposition of interfering paths. Even in the restrictive case of real, equal-valued couplings and local, time-independent control, this simple framework

is capable of universal quantum computation (2, 3) and has inspired the development of various quantum algorithms including those for spatial search (4), graph traversal (5), element distinctness (6), and formula evaluation (7). When scaled to many particles, systems that realize quantum walks further allow for rich studies of quantum information and many-body physics: controlled tunneling of many noninteracting particles maps to sampling problems of interest in complexity theory (8, 9) and the combination of interactions and itinerance underlies a broad class of condensed-matter Hubbard models (10, 11).

In this work we introduce a platform for realizing programmable quantum walks and lattice models that combines favorable properties of optical tweezers and optical lattices. We use this platform to demonstrate spatial search by continuous-time quantum walks with neutral atoms.

Because of their broad applicability, quantum walks have been realized in a number of experimental platforms, including with photons (12-14), nuclear magnetic resonance (15), matter waves (16), trapped ions (17, 18), and superconducting qubits (19, 20). Optically trapped neutral atoms are particularly amenable to realizing quantum walks (21, 22) because they allow for high-fidelity creation and detection of individual, physically identical walkers. One approach to studying quantum walks of neutral atoms is with quantum gas microscopes, which load degenerate gases containing thousands of particles into optical lattices containing thousands of sites (23, 24). Sophisticated techniques have been developed to "cookie-cut" desired initial states out of these

^{*}Corresponding author. Email: adam.kaufman@colorado.edu.

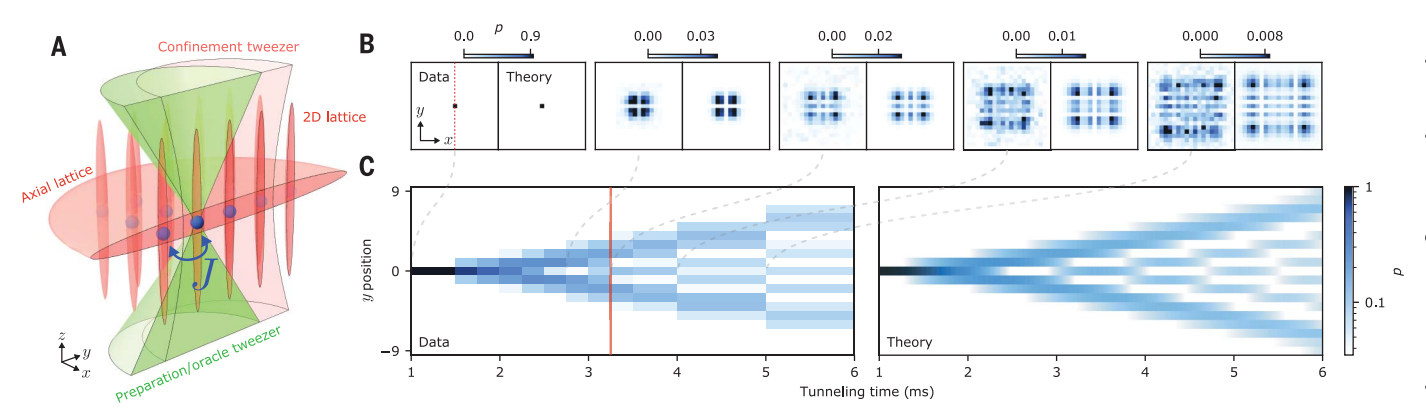


Fig. 1. Continuous-time 2D quantum walks with tweezer-implanted atoms in a lattice. (A) Individual ⁸⁸Sr atoms (solid blue sphere) are loaded and cooled in optical tweezers (preparation/oracle tweezer, green), and then implanted into single sites of a 3D optical lattice composed of a 1D crossed-beam lattice aligned along gravity (axial lattice, red half-disk), and a bowtie lattice (2D lattice, red). The 2D lattice contains more than 2000 sites that are compatible with high-fidelity imaging and ground state cooling (42) and is tunable to a regime where nearest-neighbor sites are coupled with a tunneling energy J, allowing the atoms to move through the lattice (translucent blue spheres). The preparation tweezers used to implant atoms can further be used to programmably modify the depth of individual sites in this lattice and a large-waisted tweezer (confinement tweezer, pink) can be used to apply a tunable harmonic confining potential that spans many lattice sites. (**B**) Atoms implanted in this lattice undergo continuous-time quantum walks in 2D, such that the probability density p corresponding to their measured position (left panels)

exhibits ballistic expansion and wavelike interference; this is in good agreement with theory with fitted values of the tunneling energy (right panels) up to an evolution time of 5 ms, where the atoms have coherently explored a region spanning ~200 lattice sites. Each pixel in these plots represents a single lattice site. (**C**) Tracing out the *x* axis of this 2D quantum walk yields a 1D quantum walk along the *y* axis (left panel), which is in good agreement with theory (right panel). Sampling times in these plots correspond to the leading edge of each colored region. For data to the left of the red line, multiple atoms can be implanted in different regions of the lattice for faster data collection (42). Here, each point in time is averaged over 200 repetitions of the experiment. For data to the right of the red line a single atom is implanted in the center of the lattice to avoid overlapping atomic wavefunctions and averaging over inhomogeneous regions in the lattice. Here, each point up to and including 3.5 ms is averaged over 3000 repetitions. The points at 4 and 5 ms are averaged over 6000 and 14,000 repetitions, respectively.

¹JILA, University of Colorado and National Institute of Standards and Technology, and Department of Physics, University of Colorado, Boulder, CO 80309, USA.
²Department of Computer Science, University of Maryland, College Park, MD 20742, USA. ³Institute for Advanced Computer Studies and Joint Center for Quantum Information and Computer Science, University of Maryland, College Park, MD 20742, USA.

complicated many-body states (22, 25, 26). A complementary approach is to rapidly assemble such states with optical tweezer arrays. In this case it is possible for individual atoms to be deterministically assembled into nearly arbitrary geometries (27, 28) and rapidly lasercooled to their three-dimensional (3D) motional ground state (29-35). Pioneering studies have used tweezers to explore tunneling between up to eight sites (26, 36, 37); however, such systems are sensitive to disorder, making it difficult to realize coherent itinerance across many sites. We present an alternative solution that uses optical tweezers and high-fidelity laser cooling for fast, programmable implantation and control of single atoms in a Hubbardregime optical lattice.

We use this approach to study quantum walks of individual atoms spanning hundreds of sites in a 2D lattice and to locally control those walks to realize a spatial search algorithm. In this case, elements of the search space are represented by sites in the lattice; the location of the atom, or walker, is initialized through tweezer implantation and the search oracle is created with dynamically programmable tweezers superimposed on the lattice (4). The techniques demonstrated here may advance studies of nonequilibrium and ground-state Hubbard physics, where fast cycle times, versatile state preparation, and siteresolved potentials can advance entanglementmeasurement protocols and implement certain sampling problems (8, 9, 38-40). These tools could be further extended to other types of systems, like molecules (34, 41), that are less amenable to evaporative cooling but are powerful in terms of many-body physics and quantum information.

Our experiments begin by trapping and cooling individual strontium (88Sr) atoms in optical tweezers (32). The atoms are then transferred into one 2D layer of a 3D optical lattice (Fig. 1A). This transfer need not be fully adiabatic with respect to on-site motional timescales because the tightly confining optical lattice allows for higher-fidelity optical cooling than can be performed in the tweezers, yielding a typical 3D motional ground state fraction of $100^{+0}_{-7}\%$ (42). This lattice is composed of a 1D crossed-beam lattice which is aligned along gravity and a 2D bowtie lattice. The depths of these two lattices are independently tunable and are reduced to 26.0E_R^{Ax} and $5.0E_R^{2D}$, respectively, to study tunneling after optically cooling the atoms, where \mathbf{E}_{R}^{Ax} and E_R^{2D} are the recoil energies of the two respective lattices (42). The detuning between sites in the axial lattice caused by gravity suppresses tunneling along this axis, whereas atoms tunnel freely in the 2D lattice with an average tunneling energy of $J_0/\hbar=2\pi imes 163$ Hz, corresponding to a characteristic tunneling time of $\tau = \hbar/J_0 = 0.975\,$ ms (the tunneling

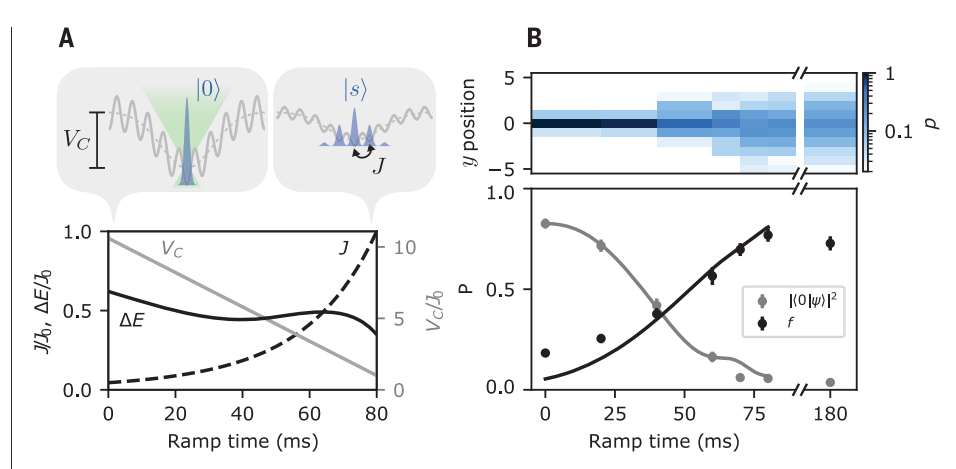


Fig. 2. Adiabatic resource state preparation. (A) An atom implanted in the site with the lowest energy in a deep lattice with no tunneling (left callout), which we label as being in state $|0\rangle$, can be adiabatically connected to the ground state |s\) of a shallow lattice with tunneling (right callout) through an adiabatic ramp of the tunneling energy (J) and the depth (V_c) of the confinement tweezer. In the callouts the gray dashed line denotes the potential provided by the confinement tweezer and the solid gray line indicates the sum of the tweezer and lattice potentials. The preparation tweezer used to initially implant the atom in $|0\rangle$ is shown schematically in green. By ramping J and V_C together we can maintain a roughly fixed energy gap ΔE between the ground and first excited states of the system throughout the ramp. (**B**) As an atom evolves under this ramp its amplitude spreads over many sites in the 2D lattice. Here, the x coordinate has been traced out for illustration purposes, showing the spread in the atom's y position (top). During this ramp, the population on the initial site (gray points) decreases and the overlap f (see main text) between the classical probability distributions corresponding to the prepared state $|\psi\rangle$ and the expected lattice ground state |s\ (black points) increases, eventually reaching 76.9(3.3)%. This is in reasonable agreement with theory (solid lines) given the independently measured parameters in our ramp, and an overall scale factor to account for filtering and loss due to imperfect preparation of the atoms in their 3D motional ground states (42). The prepared state is not observed to substantially evolve even after more than 100 tunneling times (right side of the broken axis), suggesting that it is indeed the lattice ground state. Each data point corresponds to 500 repetitions of the experiment except for the points at 70 and 180 ms which are averaged over 1500 repetitions.

energy differs slightly between the two axes of the lattice) (42).

The evolution of the system in this regime can be understood as a quantum walk on a graph where each site $|i\rangle$ in the lattice is represented by a node, and nodes corresponding to tunnel-coupled sites are connected by an edge. Such a graph can be represented by its adjacency matrix A, where $A_{ij}=0$ unless nodes i and j are connected in which case $A_{ij}=1$. Given this definition the Hamiltonian of the system is:

$$H_{
m Lat} = -J \sum_{i,j} A_{ij} |i
angle \langle j| - \sum_i V_i |i
angle \langle i| ~~~~ (1)$$

where J is the tunneling energy; we have also included a local energy shift V_i that is present as a result of the finite extent of our lattice beams (42) and can be programmably modified through two sets of optical tweezers (Fig. 1A). If the tweezers are fully extinguished, given the lattice uniformity, $|V_i| \ll J$ and this term can be disregarded. In this case, an atom implanted in one site of the lattice undergoes a continuous-time quantum walk in 2D (Fig. 1B). The evolution of this atom's wavefunc-

tion is in good agreement with the theoretical prediction for a flat lattice with constant V_i and a distant boundary, exhibiting the formation of fringes in the probability density p of the atom's measured position thanks to interference between the multiple paths by which the atom can arrive at a given site after its evolution. This is in contrast to the behavior of classical random walks, which exhibit diffusive expansion of a Gaussian probability density distribution. We can trace out one of the atom's two spatial coordinates (Fig. 1C) which, given the form of $H_{\rm Lat}$ for a 2D square lattice, results in a 1D quantum walk along the remaining axis. The resulting data are in good agreement with theory, showing the expected ballistic or light-cone-like spreading of the atomic probability density (1). For the latest time shown here of t = 5.0 ms, the probability density continues to exhibit clear interference fringes (42), suggesting that the atom has maintained phase coherence while exploring a region spanning ~200 lattice sites. At later times the atom begins to sample the inhomogeneous potential resulting from the finite extent of the lattice beams and the infinite flat lattice approximation breaks down (42).

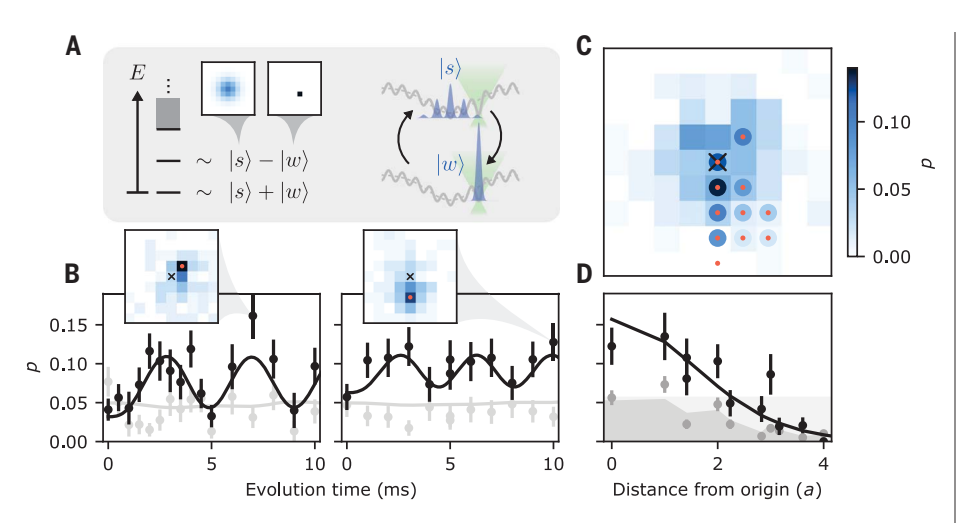


Fig. 3. Spatial search by continuous-time quantum walks. (A) When applying an oracle Hamiltonian $H_w = -V_w |w\rangle \langle w|$ through a tweezer (green) that selects for an arbitrary marked site $|w\rangle$ with appropriate strength, the spectrum of the system includes ground and first excited states that are approximately even and odd superpositions of $|w\rangle$ and the lattice ground state or resource state $|s\rangle$ (42). Consequently, evolving $|s\rangle$ under H_w results in coherent oscillations between $|s\rangle$ and $|w\rangle$. (B) Measurements of the resulting oscillations in the populations on the marked sites (black points) are in good agreement with theory, up to an overall offset, with independently characterized values of the state preparation fidelity, tunneling rate, and confinement potential (black lines) (42). For comparison we also plot the population in $|0\rangle$, at the center of the lattice (gray points and theory curves). (Insets) measured populations versus position at the peak of these oscillations where the location of the relevant oracle is marked by a red point and the lattice center by a cross. (C) The population on the marked site after a 2.46 ms guench is plotted for a selection of oracles (the lattice center is marked by a cross, and the position of each oracle by a red point, with the corresponding population shown in the surrounding circle. For comparison, the measured amplitudes in $|s\rangle$ are shown in the background). (**D**) Plotting the amplitudes from (C) as a function of oracle distance from the lattice center (black points, $a = 813/\sqrt{2}$ nm refers to lattice spacing) reveals quench behavior that is in good agreement with a theory prediction (black curve) with no free parameters (42). In a region spanning ~13 lattice sites the marked site can be found by looking for the highest amplitude site after the quench. At longer distances the amplitude on the marked site still increases from its value in |s> (theoretical and measured amplitudes in |s) shown in dark gray shading and points, respectively), but can be exceeded by the population at the origin in |s\rangle (light gray shading), limiting the size of the search space. Color scale is shared across this figure and all data points are averaged over 500 to 600 repetitions of the experiment.

This coherent exploration of Hilbert space through continuous-time quantum walks can be harnessed in a variety of quantum algorithms including those for spatial search (4). Spatial search is a specialization of the unstructured search problem with additional constraints on how the space can be explored. A continuous-time analog of Grover's search algorithm (43) performs search by quantum walk in the limiting case of a fully connected graph. The problem becomes more difficult when edges are removed from the graph, which may preclude the quadratic Grover speedup depending on the graph structure. Surprisingly, quadratic speedup can persist even for much less well connected graphs. In particular, for N-vertex square lattice graphs the search can be performed in time $O(\sqrt{N} \text{ polylog } N)$ in only four dimensions (4) whereas the full, optimal (43) quadratic speedup is recovered in five or more dimensions (4). Although the behavior of these single-particle walks can be captured by a classical wave equation involving N coupled oscillators (44), in the specific setting of searching a memory that is distributed in real space with a local probe (45), quantum walks of even a single particle can provide a notable quantum advantage (42).

In these algorithms the lack of structure in the search space suggests that a natural starting point is the uniform superposition $|S\rangle = \sum\nolimits_{i=1}^N |i\rangle/\sqrt{N} \text{ over all standard basis states in the relevant Hilbert space. Assuming periodic boundary conditions, this resource state <math display="inline">|S\rangle$ is precisely the ground state of $H_{\rm Lat}$ with constant V_i . To approximate this resource state we prepare the ground state $|s\rangle$ of $H_{\rm Lat}$ (Fig. 2) in the presence of a potential V_i provided by an extra confinement tweezer (Fig. 1A). This tweezer has a nearly Gaussian profile with a fixed waist of 5.8a, where a is the 2D

lattice spacing, and tunable overall depth

 $V_{\rm C}$. At fixed J, the lattice ground state $|{\rm s}\rangle$ is similar to $|S\rangle$ except with an approximately Gaussian envelope with a width determined by the value of $V_{\rm C}$.

To prepare the state $|s\rangle$ we implant an atom in the deepest site of the combined potential generated by the lattice and the confinement tweezer, which we label as being in state $|0\rangle$. This is the ground state of the system when the lattice is deep and $J \ll V_C$. The state $|0\rangle$ can be adiabatically connected to the ground state $|s\rangle$ in a shallow lattice through a ramp of the tunneling energy (Fig. 2A). In practice we perform a linear ramp of the lattice depth $V_{\rm L}$ as a function of time t resulting in a nonlinear ramp in the tunneling energy (42). We also ramp the depth $V_{\rm C}$ of the confinement tweezer to maintain an approximately constant value of the energy gap ΔE between the ground and first excited states during the ramp, which substantially relaxes the requirements on adiabaticity and improves the fidelity with which we can prepare $|s\rangle$. The observed evolution during this ramp is in reasonable agreement with theory (Fig. 2B), where the atoms start out primarily in $|0\rangle$ and smoothly delocalize over many sites over the course of an adiabatic ramp of V_C and J that is 80 ms in length. The prepared state $|\psi\rangle$ can be compared with $|s\rangle$ by computing the overlap between their populations, namely with the classical fidelity

$$f = \Bigl(\sum_i \sqrt{p_{\psi,i}p_{s,i}}\Bigr)^2$$
, where $p_{\psi,i}$ and $p_{s,i}$ de-

note the populations on site i in states $|\psi\rangle$ and $|s\rangle$, respectively. This yields an upper bound on the fidelity with which we have prepared $|s\rangle$ of 76.9(3.3)% but does not certify any phase coherence between the amplitudes occupying different sites. However, the prepared state is not observed to substantially evolve over more than 100 tunneling times and the adiabatic ramp can be reversed to recover 57(5)% of the atoms in $|0\rangle$ (excluding loss caused by filtering of hot atoms) (42). This suggests that $|s\rangle$ has been prepared with a fidelity of 76(3)% in agreement with the bound set by the classical fidelity; we can thus proceed with the search procedure. Note that in this work and the associated supplementary materials all confidence intervals refer to one standard error of the mean.

The central idea in quantum-walk-based search algorithms is the presence of two competing terms in the Hamiltonian: a diffusion term $H_{\rm Lat}$ corresponding to tunneling, whose ground state is $|s\rangle$, and an oracle term $H_w = -V_w|w\rangle\langle w|$, whose ground state marks a specific site $|w\rangle$. H_w can be applied to the system with variable drive strength V_w but the choice of $|w\rangle$ is unknown to the experimenter and is the quantity being searched for. Given a sufficiently connected graph and appropriate choice of V_w , the states $|s\rangle$ and $|w\rangle$ are similar in energy and coupled under the full search

Hamiltonian $H = H_{Lat} + H_w$. This results in ground and first excited states $|\pm\rangle$ that are approximately the even and odd superpositions of $|s\rangle$ and $|w\rangle$, and are separated by an energy gap $\Delta E = O(1/\sqrt{N})$, where N is the number of elements in the search space (Fig. 3A) (42). As a result quenching to this Hamiltonian from the resource state $|s\rangle$ yields coherent oscillations to $|w\rangle$ and back with a characteristic period of $O(\sqrt{N})$ that is independent of the specific choice of $|w\rangle$. Measuring the position of the walker after a half period of this oscillation identifies the marked site $|w\rangle$. This procedure can also be run backward to prepare $|s\rangle$ from an atom implanted in a predetermined site $|w'\rangle$, avoiding any additional overhead associated with adiabatic resource state preparation (42).

The choice of V_w must be carefully finetuned to minimize the energy gap between $|\pm\rangle$ given N and the connectivity of the graph (4). Here we choose $V_w = 12.55(65)J_0$, which is biased deeper than the optimal value to avoid certain sources of technical noise (42). Even with optimal V_w in a 2D square lattice with cyclic boundary conditions $|\pm\rangle$ deviate from the even and odd superpositions of $|s\rangle$ and $|w\rangle$ and the scaling of ΔE with N is modified, resulting in an asymptotic runtime of $\geq O(N/\text{polylog }N)$ (4). This scaling is further modified by the nonperiodic boundary conditions in our experiment (42). Nonetheless, upon quenching to H starting in the state $|s\rangle$, we observe coherent oscillations in the population on the marked site $|w\rangle$ for a selection of different oracles (Fig. 3B). At the peak of these oscillations the marked site is readily identified as the highest amplitude site in the lattice. Critically, the amplitudes of these oscillations are in good agreement with theory and limited in magnitude not by technical noise but rather by the expected performance of this search procedure in a 2D square lattice (42).

It should be noted that in the case of open boundary conditions or in the presence of the confinement tweezer the behavior of these oscillations is dependent on the specific position of $|w\rangle$ (42). This position-dependent behavior sets the effective size of the search space where at greater range reduced overlap between $|w\rangle$ and $|s\rangle$ yields oscillations with reduced amplitude. In our experiment, for an oracle with a distance of $\sqrt{2}a$ from the center of the confinement tweezer (the origin) the optimal evolution time after the quench is 2.46 ms. Performing this quench and evolution for a variety of different oracles (Fig. 3C), we find that the amplitude on the marked site after the evolution decreases as a function of distance from the origin, in agreement with theory (Fig. 3D). Within 2a—corresponding to a region spanning ~13 lattice sites—we can blind ourselves to the position of the oracle tweezer and identify the marked site by look-

ing for the most probable location of the walker after the quench. At longer range the amplitude at the origin after the quench and subsequent evolution can exceed that of the marked site. However, within $\sqrt{13}a$ —corresponding to a region spanning ~45 lattice sites—there is still a several-fold increase in the amplitude on the marked site relative to what was present in the resource state. This suggests that the effective size of the search space could be increased with constant overhead by measuring the amplitude of these oscillations over time. Although not demonstrated here this would help to reject any background signal that remains near the origin or effects relating to variable oscillation frequencies for different oracles.

In this work we have performed a proofof-principle demonstration of spatial search through continuous-time quantum walks of a single particle on a 2D square lattice. This is accomplished by introducing a platform that combines the programmability of optical tweezer arrays with a Hubbard-regime optical lattice which provides a clean environment for tunneling in addition to several thousand sites which are compatible with high-fidelity cooling, imaging, and coherent control (42, 46). Beyond studies with itinerance, these capabilities can also be used to prepare large, wellcontrolled ensembles of atomic qubits for quantum information, simulation, and metrology (35, 46, 47, 48, 49, 50).

In the specific context of spatial search the runtime of the algorithm demonstrated in this work does not exhibit a quadratic speedup in comparison to classical search algorithms as a result of our use of a 2D square lattice (4). A runtime of $O(\sqrt{N} \log N)$ is achievable with a single particle in such a lattice if an additional spin degree of freedom is used to implement a Dirac Hamiltonian (51) or a discrete-time quantum walk (52). This degree of freedom can be either internal to the walker or external and realized with a modified optical lattice containing an array of doublets (53). The optical clock qubit in strontium is a strong candidate for implementing this spin internally because it is well controlled (46) and long lived compared with the tunneling time (35). Moreover, it is possible to engineer state-dependent optical potentials for this qubit (54) to realize a broad class of discrete-time quantum walks (21.55).

Although there is a setting in which such single-particle quantum walks can provide a uniquely quantum advantage (45), this advantage can be extended to a broader class of problems by realizing these dynamics in a system whose state space scales rapidly with physical resources. This can be achieved by extending this work to multiple particles, where the state space and thus graph size grows exponentially with particle number (42). Given the cooling performance and singleparticle control demonstrated here such experiments could be performed with tens to hundreds of atoms, where the appropriate many-body oracle is applied through tunable Rydberg-mediated interactions (42, 46). Beyond spatial search the programmable control and assembly of large-scale itinerant systems enabled by this platform provides one route toward programmable boson sampling with many particles (8, 9) as well as the direct assembly and characterization of Hubbard models (56, 57).

REFERENCES AND NOTES

- D. Reitzner, D. Nagaj, V. Buzek, Acta Physica Slovaca 61, 603-725 (2011).
- A. M. Childs, Phys. Rev. Lett. 102, 180501 (2009)

Computing Machinery, 2003), p. 59

- A. M. Childs, D. Gosset, Z. Webb, Science 339, 791-794
- A. M. Childs, J. Goldstone, Phys. Rev. A 70, 022314 (2004). A. M. Childs et al., in Proceedings of the Thirty-Fifth Annual ACM Symposium on Theory of Computing (Association for
- A. Ambainis, in 45th Annual IEEE Symposium on Foundations of Computer Science (IEEE Computer Society, 2004),
- E. Farhi, J. Goldstone, S. Gutmann, Theory Comput. 4, 169-190 (2008).
- S. Aaronson, A. Arkhipov, in Proceedings of the Forty-Third Annual ACM Symposium on Theory of Computing (Association for Computing Machinery, 2011), pp. 333-342.
- G. Muraleedharan, A. Miyake, I. H. Deutsch, New J. Phys. 21,
- 10. P. A. Lee, N. Nagaosa, X.-G. Wen, Rev. Mod. Phys. 78, 17-85 (2006)
- 11. I. Bloch, J. Dalibard, W. Zwerger, Rev. Mod. Phys. 80, 885-964 (2008).
- 12. A. Peruzzo et al., Science 329, 1500-1503 (2010).
- 13. A. Schreiber et al., Phys. Rev. Lett. 104, 050502 (2010).
- 14. L. Sansoni et al., Phys. Rev. Lett. 108, 010502 (2012).
- 15. C. A. Ryan, M. Laforest, J. C. Boileau, R. Laflamme, Phys. Rev. A 72, 062317 (2005).
- 16. E. J. Meier, F. A. An, B. Gadway, Phys. Rev. A 93, 051602 (2016).
- H. Schmitz et al., Phys. Rev. Lett. 103, 090504 (2009).
- 18. F. Zähringer et al., Phys. Rev. Lett. 104, 100503 (2010).
- 19. Z. Yan et al., Science 364, 753-756 (2019)
- 20. M. Gong et al., Science 372, 948-952 (2021).
- 21. M. Karski et al., Science 325, 174-177 (2009).
- 22. P. M. Preiss et al., Science 347, 1229-1233 (2015).
- 23. W. S. Bakr, J. I. Gillen, A. Peng, S. Fölling, M. Greiner, Nature 462, 74-77 (2009).
- 24. J. F. Sherson et al., Nature 467, 68-72 (2010).
- 25. C. Weitenberg et al., Nature 471, 319-324 (2011).
- 26. B. M. Spar, E. Guardado-Sanchez, S. Chi, Z. Z. Yan, W. S. Bakr, Phys. Rev. Lett. 128, 223202 (2022).
- 27. M. Endres et al., Science 354, 1024-1027 (2016)
- 28. D. Barredo, S. de Léséleuc, V. Lienhard, T. Lahaye, A. Browaeys Science 354, 1021-1023 (2016). 29. A. M. Kaufman, B. J. Lester, C. A. Regal, Phys. Rev. X 2, 041014
- (2012).30. X. Li, T. A. Corcovilos, Y. Wang, Phys. Rev. Lett. 108, 103001
- (2012).31. J. D. Thompson, T. G. Tiecke, A. S. Zibrov, V. Vuletić,
- M. D. Lukin, Phys. Rev. Lett. 110, 133001 (2013).
- 32. M. A. Norcia, A. W. Young, A. M. Kaufman, Phys. Rev. X 8, 041054 (2018).
- 33. A. Cooper et al., Phys. Rev. X 8, 041055 (2018).
- 34. L. R. Liu et al., Phys. Rev. X 9, 021039 (2019).
- 35. A. W. Young et al., Nature 588, 408-413 (2020).
- 36. A. M. Kaufman et al., Science 345, 306-309 (2014)
- 37. S. Murmann et al., Phys. Rev. Lett. 114, 080402 (2015).
- 38. A. J. Daley, H. Pichler, J. Schachenmayer, P. Zoller, Phys. Rev. Lett. 109, 020505 (2012).
- 39. A. M. Kaufman et al., Science 353, 794-800 (2016).
- 40. A. Elben, B. Vermersch, M. Dalmonte, J. I. Cirac, P. Zoller, Phys. Rev. Lett. 120, 050406 (2018).
- 41. L. Anderegg et al., Science 365, 1156-1158 (2019)
- 42. See supplementary materials.
- 43. E. Farhi, S. Gutmann, Phys. Rev. A 57, 2403-2406 (1998).

- 44. L. K. Grover, A. M. Sengupta, Mathematics of Quantum Computation (CRC Press, 2002).
- 45. S. Aaronson, A. Ambainis, in 44th Annual IEEE Symposium on Foundations of Computer Science (IEEE Computer Society, 2003), pp. 200-209.
- 46. N. Schine, A. W. Young, W. J. Eckner, M. J. Martin, A. M. Kaufman, Nat. Phys. 18, s41567-022-01678-w (2022).
- 47. H. Levine et al., Phys. Rev. Lett. 123, 170503 (2019).
- 48. T. M. Graham et al., Phys. Rev. Lett. 123, 230501 (2019).
- 49. S. Ebadi et al., Nature 595, 227-232 (2021).
- 50. P. Scholl et al., Nature 595, 233-238 (2021).
- 51. A. M. Childs, J. Goldstone, Phys. Rev. A 70, 042312
- 52. A. Ambainis, J. Kempe, A. Rivosh, in Proceedings of the Sixteenth Annual ACM-SIAM Symposium on Discrete Algorithms (Society for Industrial and Applied Mathematics, 2005), pp. 1099-1108.
- 53. A. M. Childs, Y. Ge, Phys. Rev. A 89, 052337 (2014).
- 54. A. Heinz et al., Phys. Rev. Lett. 124, 203201 (2020).
- 55. T. Kitagawa, M. S. Rudner, E. Berg, E. Demler, Phys. Rev. A 82, 033429 (2010).

- 56. S. Onari, R. Arita, K. Kuroki, H. Aoki, Phys. Rev. B. 70, 094523 (2004). T. Ohgoe, T. Suzuki, N. Kawashima, *Phys. Rev. B.* **86**, 054520
- (2012).
- 58. A. W. Young, W. J. Eckner, N. Schine, A. M. Childs, A. M. Kaufman, Tweezer-programmable 2D quantum walks in a Hubbard-regime lattice, Version 1, Zenodo (2022); https://zenodo.org/record/6519158#.YuGMO3bMI2w.

ACKNOWLEDGMENTS

We acknowledge fruitful discussions with E. Knill, S. Geller, and M. O. Brown. We further thank A. M. Rey, K. Kim, S. Geller, and P. M. Preiss for close readings of the manuscript. Funding: This work was supported by the AFOSR (FA95501910079), ARO (W911NF1910223), the National Science Foundation Physics Frontier Center at JILA (1734006), and NIST. A.M.C. received support from the National Science Foundation (grant CCF-1813814 and QLCI grant OMA-2120757) and the Department of Energy, Office of Science, Office of Advanced Scientific Computing Research, Accelerated Research in Quantum Computing program. W.J.E. and N.S. acknowledge support from the NDSEG fellowship program, and the NRC research associateship

program, respectively. Author contributions: A.W.Y., W.J.E., N.S., and A.M.K. contributed to developing the experiments. All authors contributed to analysis of the results and preparing the manuscript. Competing interests: The authors declare no competing interests. Data and materials availability: Experimental data and code used in this work are available on Zenodo (57). License information: Copyright © 2022 the authors, some rights reserved; exclusive licensee American Association for the Advancement of Science. No claim to original US government works. https://www.sciencemag.org/about/science-licensesiournal-article-reuse

SUPPLEMENTARY MATERIALS

science.org/doi/10.1126/science.abo0608 Materials and Methods Supplementary Text Figs. S1 to S8 Table S1 References (59-77)

Submitted 31 January 2022; accepted 8 July 2022 10.1126/science.abo0608



Tweezer-programmable 2D quantum walks in a Hubbard-regime lattice

Aaron W. YoungWilliam J. EcknerNathan SchineAndrew M. ChildsAdam M. Kaufman

Science, 377 (6608), • DOI: 10.1126/science.abo0608

Combining lattices and tweezers

Optical lattices have been used as a platform for quantum simulation for the past two decades. More recently, arrays of optical tweezers, which have the advantage of rapid reconfigurability, have risen to prominence. Young *et al.* combined these tools to perform large-scale quantum walks of strontium-88 atoms prepared in optical tweezers and then implanted into the sites of an optical lattice. The combined platform holds promise for applications in quantum science. —JS

View the article online

https://www.science.org/doi/10.1126/science.abo0608

https://www.science.org/help/reprints-and-permissions

Use of this article is subject to the Terms of service